Optical and Quasi-Optical Analysis of System Components for a Far-Infrared Space Interferometer

C. Bracken[a], C. O'Sulllvan[a], A. Donohoe[a], A. Murphy[a], G. Savini[b], R. Juanola-Parramon[b], N. Baccichet[b], A. Guisseau[b], P. Ade[c], E. Pascale[c], L. Spencer[c], I. Walker[c], K. Dohlen[d], J. Lightfoot[e], W. Holland[e], M. Jones[f], D. D. Walker[f], A. McMillan[f],
[a]Dept. of Experimenatl Physics, National University of Ireland, Maynooth, Ireland
[b]Dept. of Physics and Astronomy, University College London, UK
[c]School of Physics and Astronomy, Cardiff University, UK
[d]Laboratoire d'Astrophysique de Marseille (LAM), Marseille, France
[e]Science and Technology Facilities Council (STFC), UK
[f]Glyndwr University, UK

ABSTRACT

Many important astrophysical processes occur at wavelengths that fall within the far-infrared band of the EM spectrum, and over distance scales that require sub-arc second spatial resolution. It is clear that in order to achieve sub-arc second resolution at these relatively long wavelengths (compared to optical/near-IR), which are strongly absorbed by the atmosphere, a space-based far-IR interferometer will be required. We present analysis of the optical system for a proposed spatial-spectral interferometer, discussing the challenges that arise when designing such a system and the simulation techniques employed that aim to resolve these issues. Many of these specific challenges relate to combining the beams from multiple telescopes where the wavelengths involved are relatively short (compared to radio interferometry), meaning that care must be taken with mirror surface quality, where surface form errors not only present potential degradation of the single system beams, but also serve to reduce fringe visibility when multiple telescope beams are combined. Also, the long baselines required for sub-arc second resolution present challenges when considering propagation of the relatively long wavelengths of the signal beam, where beam divergence becomes significant if the beam demagnification of the telescopes is not carefully considered. Furthermore, detection of the extremely weak far-IR signals demands ultra-sensitive detectors and instruments capable of operating at maximum efficiency. Thus, as will be shown, care must be taken when designing each component of such a complex quasioptical system.

Keywords: FISICA, far-infrared (far-IR), interferometry, double-Fourier,

1. INTRODUCTION

Over the last few years there have been impressive advances made in our understanding of both the local Universe and the distant Universe at far-IR wavelengths. Such advances come from the unprecedented combination of spectral coverage and sensitivity of the ESA Herschel Space Observatory, and the NASA Spitzer Space Telescope [1], [2], [3], [4], for example. Further improvements in sensitivity are likely to come from the proposed ESA/JAXA SPICA (SPace Infrared telescope for Cosmology and Astrophysics) mission, currently under consideration [5]. However, it generally comes as a surprise when one considers that the highest spatial resolution at far-IR wavelengths, achieved to date, is not much better than that achieved by Galileo with his optical telescopes around 400 years ago. For these relatively long far-IR wavelengths, in order to achieve the sub-arc second spatial resolution that is now possible at optical, radio, and mm/sub-mm wavelengths, a space based interferometer will be required. This requirement is simply a result of the diffraction limit described by (1), meaning that at a wavelength of 200 μm, for example, a spatial resolution of even 1 arc second would require a telescope main mirror with a diameter, D, of 50 m. This is practically unfeasible for a space-based system, especially when one considers that the optics for far-IR systems need to be typically cooled to temperatures of just a few Kelvin. Thus, if resolutions of less than 1 arc second are to be reached, then an aperture of 50 m or greater must be synthesized using aperture synthesis, where the beams of multiple telescopes, separated by large

Terahertz, RF, Millimeter, and Submillimeter-Wave Technology and Applications VIII,
edited by Laurence P. Sadwick, Tianxin Yang, Proc. of SPIE Vol. 9362, 93620N
 · doi: 10.1117/12.2076385

baselines, are combined at a central hub space craft. High spectral resolution, then, can also be achieved using one of a number of spectrometric techniques, with the one selected in this case being far-IR Fourier transform spectroscopy (FTS). This combination of Fourier transforming the data of the sampled points in the u-v plane to obtain high resolution spatial information, and then introducing a delay line into one of the beam paths where the Fourier transform of this data results in high resolution spectral information, has become known as Double-Fourier spatio-spectral interferometry (see [6], for example).

$$\theta = 1.22\frac{\lambda}{D} \tag{1}$$

FISICA (Far-Infrared Space Interferometer Critical Assessment) is a three year study aimed at designing a spatio-spectral double-Fourier interferometer concept that would be capable of answering some of the most important astrophysical questions such as how do planet and star systems form from protostellar disks, how did high-redshift galaxies form, merge and evolve into the types of galaxies we see in the local cosmological era, and how common are the molecule building blocks of life in the local Universe. The FISICA project involves an international collaboration of researchers including leaders in the fields of far-IR astronomy, cosmology, far-IR instrumentation, optics, optical materials manufacture, and satellite positioning. FISICA seeks to identify the scientific questions related to such high spatial resolution far-IR observations, and to translate these questions into a technological definition of a far-IR space-based mission, including a baseline telescope design.

The work of the FISICA group builds on previous far-IR Double Fourier studies carried out by both European and US institutes, including a candidate NASA Origins Probe mission: the Space Infrared Interferometric Telescope (SPIRIT) study [7], and the ESA Far Infrared Interferometer (FIRI) Technology Reference Study (TRS) [8]. Papers relating to issues such as metrological problems and system requirements for interferometric observations from space have already resulted from the work of the FISICA study [9]. It is the telescope design and analysis that is presented in this paper, with attention given to some of the optical design problems specific to long baseline interferometry at such short wavelengths.

2. TELESCOPE DESIGN

2.1 Telescope Baseline Design

The main goal of the light collecting telescopes, besides collecting photons from the source, is to de-magnify the beam and to propagate it across a variable distance of up to 50 m, where the beam then enters a hub spacecraft within which it is combined with the signal from the second light collector. A flat mirror oriented at 45° to the primary mirror is used to steer the de-magnified beam toward the hub, as shown in Figure 1. The signals are of course further processed in the hub through beam splitters, filters, etc., and finally absorbed by the detectors. Somewhat different to focusing telescopes, the purpose of the light collecting telescopes in this instance is to convert a parallel beam into another parallel beam, but with a compressed (or de-magnified) beam width. However, the same desire to maintain a low level of aberration and good imaging properties still exists for such a de-magnifying system. Also, sensitivity requirements calculated as part of the FISICA study call for light collecting telescopes with primary mirror diameters of 2 m.

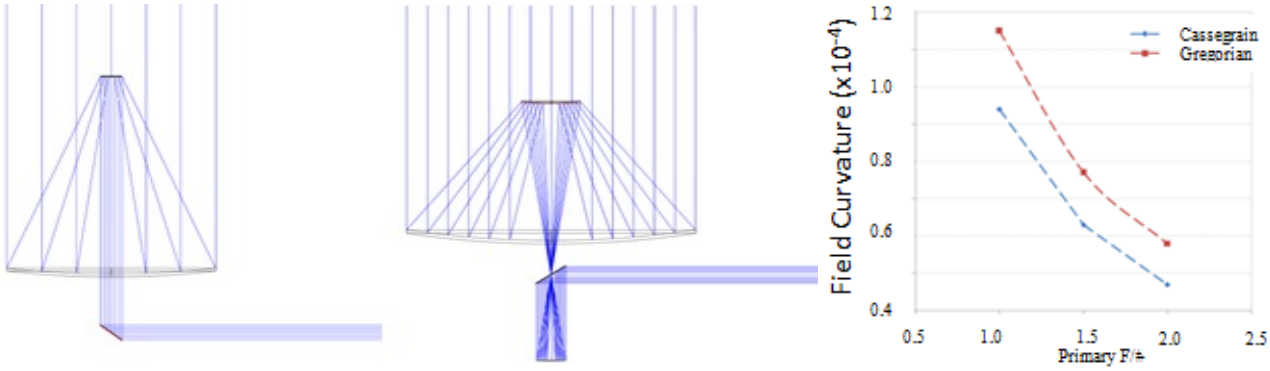

Figure 1. *left*: a Cassegrain format light collecting telescope considered for the FISICA baseline design (F/1.0). *middle*: one of the other Cassegrain formats that was also considered (F/0.5) where an extra mirror is used. As well as reducing aberration, another benefit of the extra mirror is the introduction of an intermediary focus, which may be useful for a direct imaging option to be included. *Right*: level of spherical aberration for various Cassegrain and Gregorian designs.

As a first investigation into which particular optical layout would be the best selection for a FISICA-like system, a range of designs were modelled using the ray tracing analysis package Zemax [10]. On-axis vs. off-axis layouts, Cassegrain vs. Gregorian, and two mirror vs. more than two mirror designs were compared in a trade-off analysis. The results of the analysis showed that Cassegrain designs produce lower aberrations than Gregorian designs, and on-axis designs were more favourable than off-axis designs, as expected. Also, increasing the F/# further reduced aberrations, as did the inclusion of more mirrors, but at the expense of compactness and weight, respectively, which are both clearly important for a space based system. Ultimately, such a system will require a compromise between wavefront quality and compactness/low mass. Figure 1 (right) shows an example of a comparison of aberration for both a Cassegrain and Gregorian optical format, where field curvature is plotted as a function of increasing F/#. Based on such trade-off analyses a baseline design was decided upon, namely an on-axis Cassegrain (parabolic primary and parabolic secondary) with a primary mirror of F/1.5 and a de-magnification of $m = 10$.

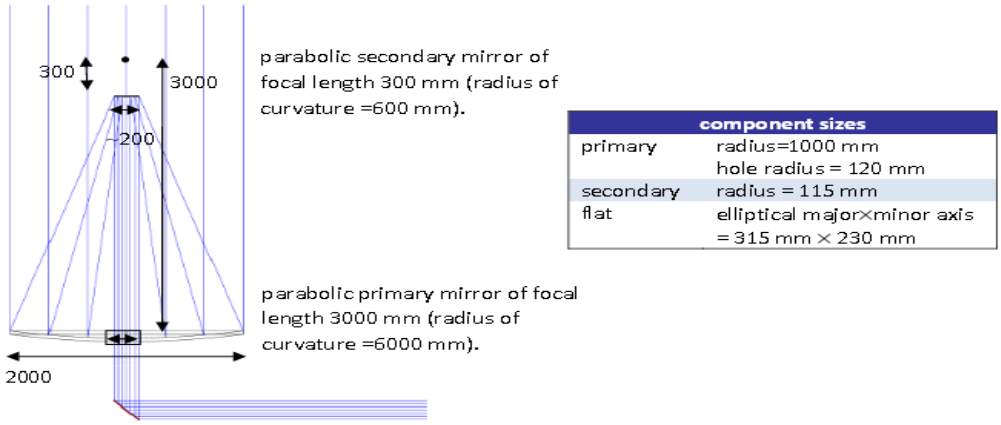

Figure 2. The current baseline optical design of the light collecting telescopes for the far-IR space interferometer. It is a Cassegrain design with F/1.5, giving a balance between low aberration and compactness.

The current chosen design, described above, was selected based on a ray tracing simulation approach. Due to the long wavelengths being considered for the far-IR space interferometer, a full physical optics (PO) analysis is also currently being carried out, the results of which may lead to an alternative optical design. For example, the PO results may suggest an off-axis design if strong wavelength dependent diffraction due to the central obscuration (secondary mirror) is observed. Figure 3 shows the results of PO simulations for a number of on-axis Cassegrain designs, where both F/# and m were varied. As can be seen, de-magnifying the beam before propagation across the large 50 m baseline produces a relatively narrow beam at the hub. However, too large a de-magnification value ($m = 15$) sees a wider beam at the hub. This is due to diffraction beginning to dominate, meaning that if the beam is condensed too much it will diverge as it propagates. This increase in beam divergence due to beam de-magnification can be thought of as the opposite of beam expanding optics, which is often used in combination with a laser in order to keep the beam collimated as it propagates.

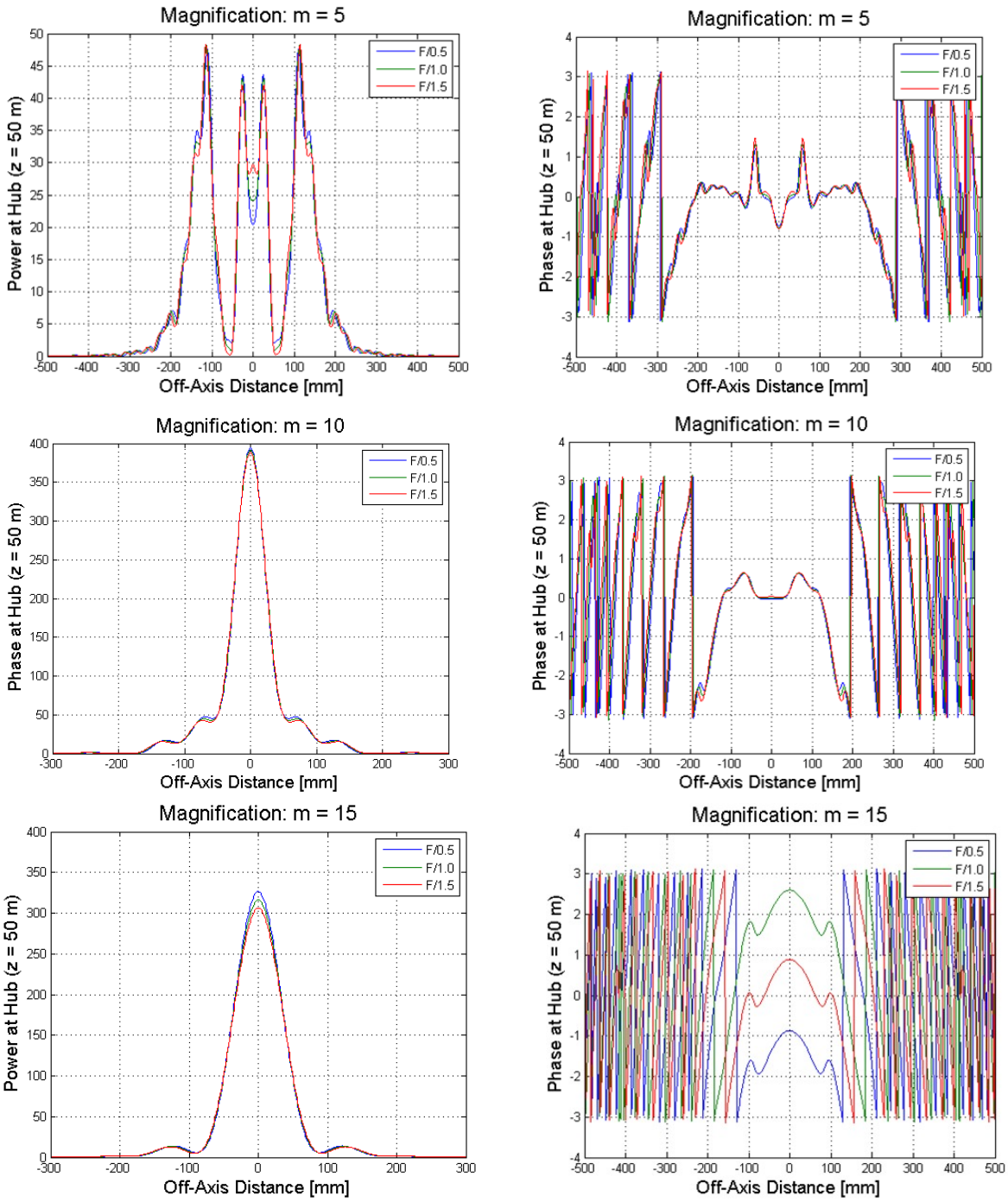

Figure 3. PO analysis of various on-axis Cassegrain optical formats, where the beam from the 2 m primary mirror was de-magnified before propagation across a distance of 50 m ($\lambda = 200$ μm). The results show the intensity and phase of the field at the hub for three different de-magnification values, $m = 5$, $m = 10$, and $m = 15$, with three values of F/# for each value of m.

What is interesting to note about the above plots is that for the smallest de-magnification value $m = 5$ the beam has not reached the far-field at a propagation distance of $z = 50$m, whereas for $m = 10$ and $m = 15$ the intensity patterns do resemble far-field patterns. A quick verification of this can be obtained from calculation of the Fresnel number (2) for each case. If $F < 1$ the beam is said to be in the far-field and will exhibit Fraunhofer diffraction [11], and if $F \geq 1$ the beam is either in the near-field, or else not quite in the far-field (F slightly greater than 1), and will exhibit Fresnel diffraction [12], [13].

$$F = \frac{a^2}{L\lambda} \tag{2}$$

Table 1. Fresnel number for various de-magnified beams after propagation over 50 m.

L = 50 m and λ = 200 µm			
m = 5	a = 0.2 m	F = 4.0	Near-field
m = 10	a = 0.1 m	F = 1.0	Nearly Far-field
m = 15	a = 0.067 m	F = 0.44	Far-field

2.2 De-magnification of primary beams

FISICA's two light collecting telescopes collect the light incident from the sky, but from two distinct sections of the wavefront as shown in Figure 4. The collected light is then redirected as near-collimated beams to the beam combining optics in the interferometer hub that is positioned midway between the two light collectors. While sensitivity requirements demand that the light collectors will have large main mirror diameters of 2 m, the beam size at the aperture of the hub optics needs to be minimized (thus minimizing the thermal mass which must be actively cooled), leading to the initial assumption to employ a large demagnification value (m). However, due to the long wavelength of the far-IR signal beams, diffraction effects become significant and large beam divergence can result if the beam widths are compressed too much, leading to beams with large optical surface areas at the hub aperture. Furthermore, demagnification of the primary beam correspondingly magnifies off-axis field angles, again resulting in large beams at the hub if the value of m is set too high.

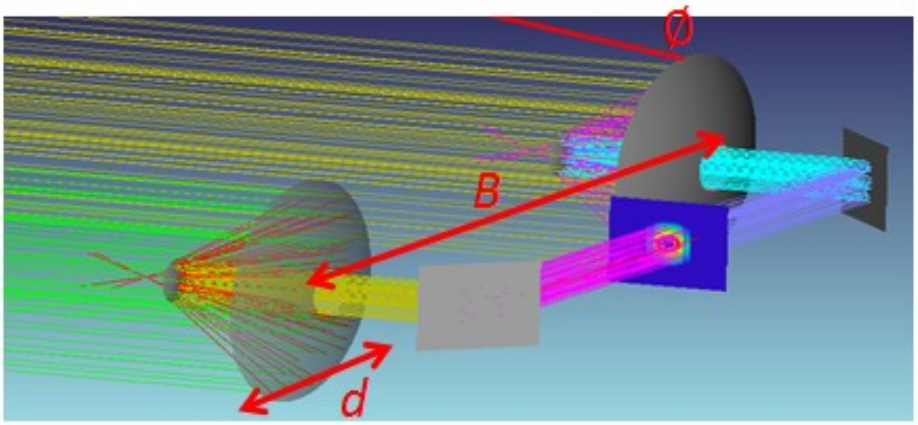

Figure 4. The two light collecting telescopes, sampling two sections of the wavefront and then redirecting the beams at 45° to the central hub, represented here simply as a square. d = 2 m, B = 2 – 50 m, and ϕ = ±0.5'.

2.1.1 Gaussian beam approximation

As a first approach to optimizing the de-magnification value of the two collecting telescopes, the beam from each of the telescopes was approximated as a Gaussian of beam width w, where w is a function of propagation distance z, and is described by (3) [14].

$$w(z) = w_o \sqrt{1 + \left(\frac{\lambda . z}{\pi . w_o^{\,2}} \right)^2} \tag{3}$$

where λ is the wavelength of the light, and w_o is the radius of the de-magnified beam before propagation over the length of the baseline. A propagation distance of 50 m, corresponding to the maximum baseline, was modelled for varying initial beam width values, where λ was set to 200 µm since beam divergence will be clearly be more severe at the longer wavelengths. Figure 5 shows the predicted results, where the minimum possible value for the beam waist at the hub is 79.8 mm, corresponding to a beam at the collector telescope with a beam waist radius of w_o = 56.4 mm, or beam diameter of 112.8 mm.

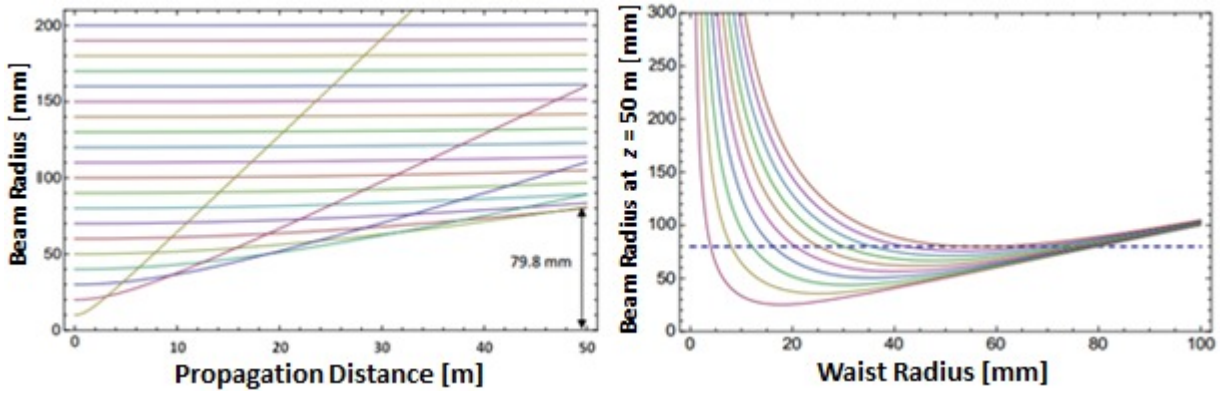

Figure 5. *left*: Beam radius as a function of propagation distance for different beam waists at collecting telescopes for λ=200 μm, and *right*: output waist radius at hub telescope for maximum baseline of z = 50 m for various wavelengths ranging from 20-200 μm (in steps of 20 μm). The upper most curve corresponds to 200 μm, and the lowest curve corresponds to 20 μm.

If we then consider that the field intercepted by the primary mirror can be represented by a uniform disk of radius a = 1 m, and that the best fit Gaussian to a uniform disk of radius a has a beam radius of 0.892a, then the best fit Gaussian to a primary mirror of radius = 1 m has a beam radius of 0.892 m. Based on this Gaussian beam approximation, then, the optimum de-magnification power for the light collecting telescopes is m = 892/56.4 = 15.8.

2.1.2 Off-axis beams

The ideal de-magnification of m = 15.8, described above, was calculated for on-axis beams only. However, the relatively large field of view required by a FISICA type system means that rays off-bore sight should be also be considered in the analysis. The analysis of these off axis rays at angles of θ is particularly important as demagnification by a factor of m will result in the de-magnified rays propagating across the baseline at angles of $m.\theta$, which will clearly lead to large hub beams if m is too large. The baseline field of view for FISICA is 1' x 1', so a similar Gaussian beam analysis to that described above was carried out for beams incident on the primary (before de-magnification) at angles of ±0.5'. Figure 6 shows the minimum beam waist that can be achieved at the hub for increasing de-magnifications and for a variety of wavelengths. When both diffraction and off-axis rays are taken into account for a wavelength of λ = 200 μm, we find that the minimum beam waist that can be achieved at the hub for the maximum baseline of 50 m is about 169 mm, which corresponds to a de-magnification of m = 11 (Figure 3 - left). The right side of Figure 3 also shows that if a larger field of view is to be employed, or if a larger wavelength range is demanded (up to 400 μm), then a smaller value for m will be required if the bam width at the hub is to be minimized.

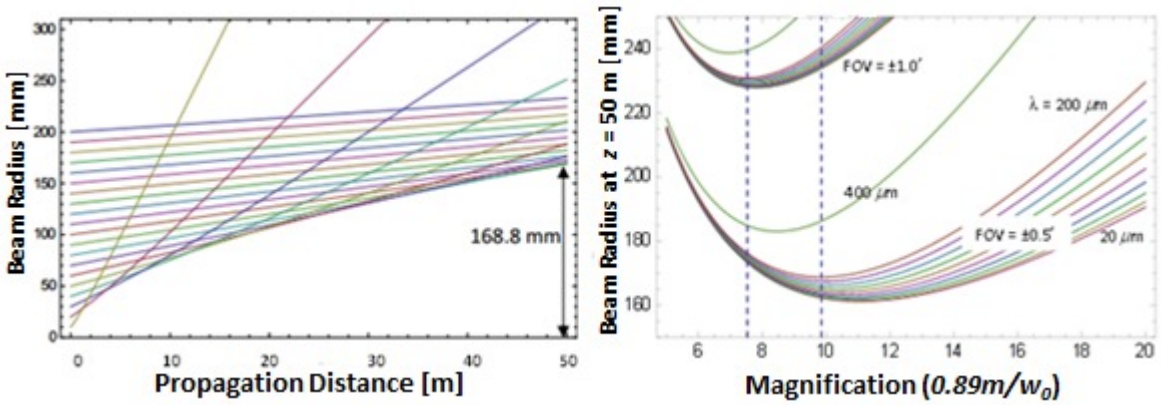

Figure 6. *left*: Beam radius as a function of propagation distance for different beam waists at collecting telescopes for λ=200 μm, including off-axis beams at ±0.5', and *right*: output waist radius at hub telescope for maximum baseline of z = 50 m for various wavelengths ranging from 20-200 μm (in steps of 20 μm) and increasing de-magnification, again including the off-axis beams. λ=400 was also simulated, as well a larger FOV of ±1.0', both of which give rise to much larger hub beams.

3. MIRROR SURFACE ACCURACY

3.1 Surface form errors

Every telescope mirror will inevitably exhibit some level of surface from errors and surface roughness. Surface form errors can either be the result of manufacturing inaccuracies, or can be introduced post-manufacturing when thermal stress, gravity, or wind (if inside an atmosphere) can cause the mirror surface to deform from its ideal shape [15], thus yielding aberrations on the wavefront. Such aberrations not only reduce imaging quality, which is the case with single telescope systems, but also lead to reduced interferometric visibility when the beams of multiple telescopes are coherently combined. In fact the effect of these aberrations on interferometric (or fringe) visibility becomes significant for even very small surface form errors when dealing with the relatively short wavelengths of the far-IR band. Furthermore, there are quite strict visibility requirements set by both the FIRI study [16] and SPIRIT study [17], where V = 94% in both cases. This required visibility of 94%, or error budget of 1 - V = 6%, is then broken down further to separately budget for errors due to wavefront tilt, pupil shift, etc., as well as optical aberrations. The FIRI report allows for a loss of 0.0031 specifically for optical aberrations, whereas the SPIRIT report allows only a 0.0025 loss for the same aberrations, where the wavelength in both cases is taken to be 25 μm. It is the more strict SPIRIT value that is used as a reference visibility requirement for the analysis shown is this study.

As a first attempt to model the effects of aberrations on fringe visibility, the two wavefronts with diameters of 2 m (corresponding to the 2 m primary mirrors) were approximated as uniform disks sampled as a set of complex points corresponding to amplitude and phase. If the two disks are coherently summed, and then a variable optical path difference (OPD) is introduced into one of the disks, then the resulting sum would be expected to produce a well-defined fringe pattern corresponding to complete constructive interference for OPD = 0, 2π, 4π, ..., and complete destructive interference for OPD = π, 3π, 5π, ... If the wavefront disks are normalised then complete constructive interference will give a result of 1 + 1 = 2, and complete destructive interference will of course be 0. The interferometric visibility then can be calculated using (4).

$$V = \frac{I_{\max} - I_{\min}}{I_{\max} + I_{\min}} \tag{4}$$

If an aberration is then introduced into one or both of the wavefronts, and the visibility is again calculated, it will be found that $V < 1$ since there will no longer be complete constructive or destructive interference. General surface form errors will be some combination of spherical aberration, astigmatism, coma, etc., and appropriate Zernike functions Z_n^m can be used to describe each particular type, as shown in Figure 7 (right). The surface form error analysed in the example for this paper was purely astigmatism Z_2^2 (5), however similar analysis could be applied to any type of aberration.

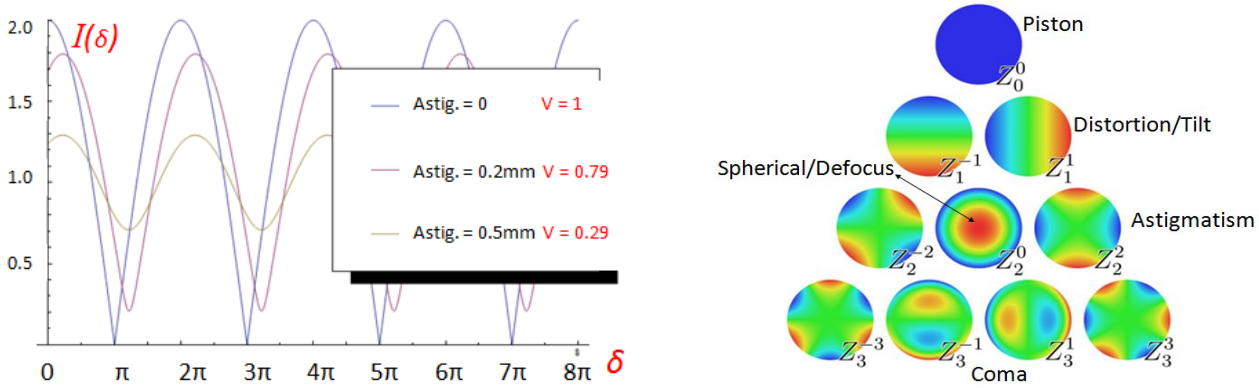

Figure 7. *left*: The effect of reduced visibility due to astigmatic aberration on one of the two wavefronts, and *right*: how some other common aberrations can be represented by the Zernike polynomials.

By setting the visibility to be $V \geq 0.9925$, a limit on the maximum level of astigmatism was calculated (for λ = 25 μm). It was found that there could be no more than σ = 418 nm astigmatic error (corresponding to α = 0.172) on a 2 m diameter wavefront, where σ is the maximum edge deviation from zero mean (along the axis of aberration). The maximum allowed size of σ scales linearly with wavelength, so the visibility becomes more forgiving at the other end of the waveband (about 3.34 μm at λ = 200 μm).

$$Z_2^2 = \alpha\sqrt{6}(\cos^2\theta - 0.5)\rho^2 \tag{5}$$

$$\sigma = \frac{2\alpha}{k}\sqrt{6}(\cos^2\theta - 0.5)\rho^2 \tag{6}$$

In (6) k is the spatial frequency (or wave number), and the factor 2 is included to account for both the forward and reflected paths of the beam.

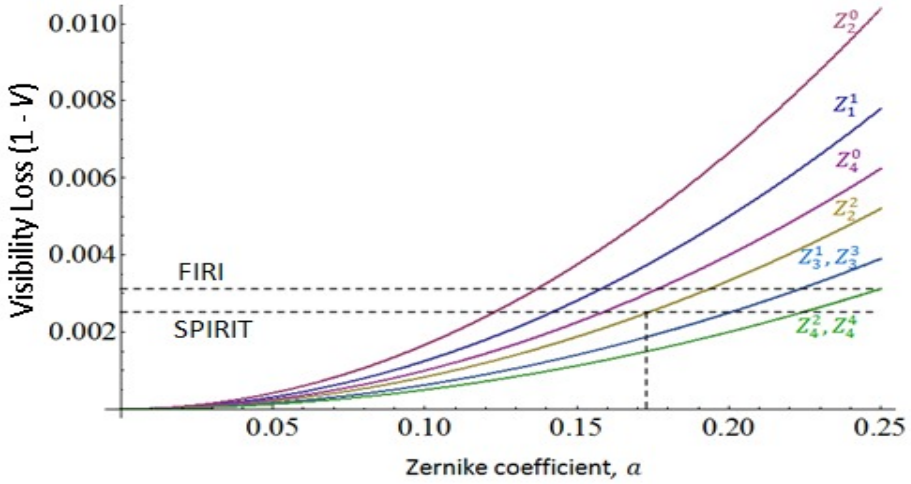

Figure 8. The effect of mirror surface form errors, expressed as Zernike functions, on interferometric visibility. The dotted lines show the cut-off (maximum) for both the FIRI [13] and SPIRIT [14] analyses.

3.2 Surface roughness

As well as analysing surface form errors, random surface roughness was also modeled in order to examine its effect on fringe visibility. Mirror surface roughness is related to wavefront errors which affect the image Strehl ratio (the ratio of peak diffraction intensities of an aberrated wavefront to those of a perfect wavefront). Random surface errors were first described by Ruze in 1966 [18], so these errors are often referred to as "Ruze errors". The primary effect of such surface errors is to scatter power from the main beam into a wide scatter pattern and thus add power to the side-lobes of the beam pattern. The total beam pattern, then, can be written as a sum of the error-free antenna/mirror beam pattern I_{FF} and the error (or Ruze) beam I_R, as shown in (7).

$$I(\theta) = I_{FF}(\theta) + I_R(\theta, \varepsilon) \tag{7}$$

While moderately sized surface errors did not significantly affect the beam pattern of a 2 m diameter main mirror, they did affect the visibility quite significantly (as was the case with the Zernike errors). The surface errors also reduced beam efficiency to some extent. The right side of Figure 9 shows that if the allowed visibility loss is again held to the value set by the SPIRIT study (budget for surface errors), then random surface errors of about $\lambda/175$ can be tolerated across one primary mirror, or $\lambda/255$ across two primary mirrors if no correlation is assumed between the errors of one mirror with the other. Thus, for a wavelength of λ = 25 μm, $\varepsilon \leq 143$ nm for one mirror, and $\varepsilon \leq 98$ nm for two mirrors.

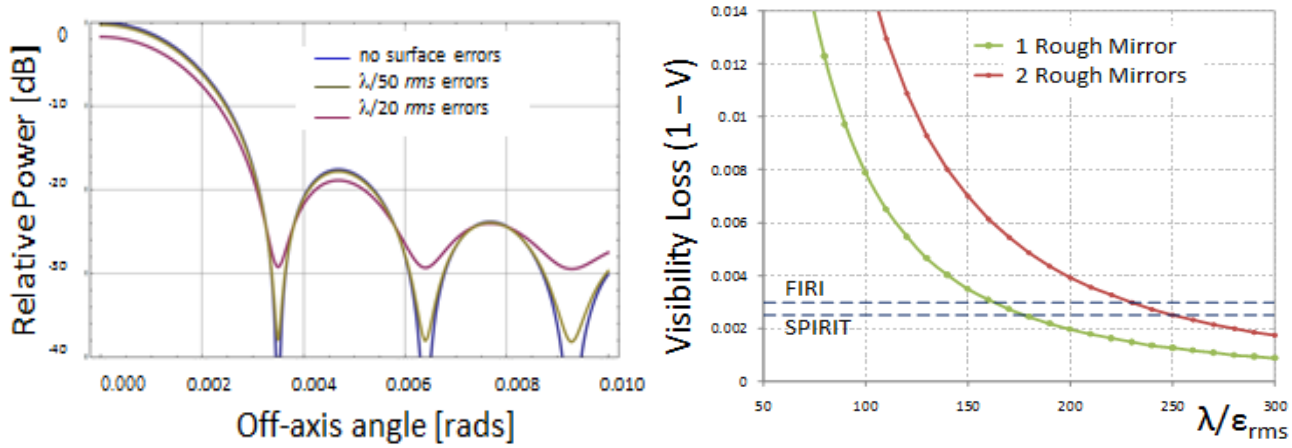

Figure 9.The effect of random surface errors on primary mirror beam pattern (*left*), and on interferometric visibility (*right*). The dotted lines show the cut-off (maximum) for both the FIRI [16 FIRI] and SPIRIT [17 Hyde] reference values.

4. TESTBEDS AND INSTRUMENT SIMULATOR

4.1 Double Fourier testbeds

In support of furthering the development of the technology and measurement techniques that will be required to realise a space-based double Fourier spatio-spectral interferometer, a number of testbed activities are currently under study as part of the FISICA project [19]. Both University College London and Cardiff University have double-Fourier testbeds under experiment, with Maynooth University and the University of Lethbridge also providing support to the studies. The aim of the testbed research is to use the double Fourier technique to reproduce the spectral and spatial distributions of a number of test sources, and in the process to understand the issues that can arise with such complex measurements.

The testbed modeling carried out by Maynooth University is aimed at unravelling the inefficiencies that can creep into such sensitive systems, and ultimately to help optimise the testbeds. An example of such an issue is illustrated in Figure 10 (right). During a series of measurements it was realized that there was a significant level of loss in the Cardiff testbed which was dependent on the optical path length of the spectral arm. Computational modelling of the system helped to determine that the most likely cause of loss was misalignment of the roof mirror (bottom of Figure 10 (left)). Tilting of the mirror by as little as half a degree gave rise to losses of up to 40%. As a result a more robust roof mirror was employed in the new testbed system, where the angles of the mirror can be more accurately controlled.

Figure 11 shows how a beam can be tracked through the full optical path of the testbed, in this case propagating from the detector through to the primary mirror (as opposed to propagating from primary mirror to detector, as was the case in the previous examples). It is clear that the beam is well controlled for wavelengths up to 90 μm, with a small level of spill over at the primary mirror for a wavelength of 300 μm. Extending the wavelength to 2 mm clearly introduces significant diffraction effects that will lead to large losses.

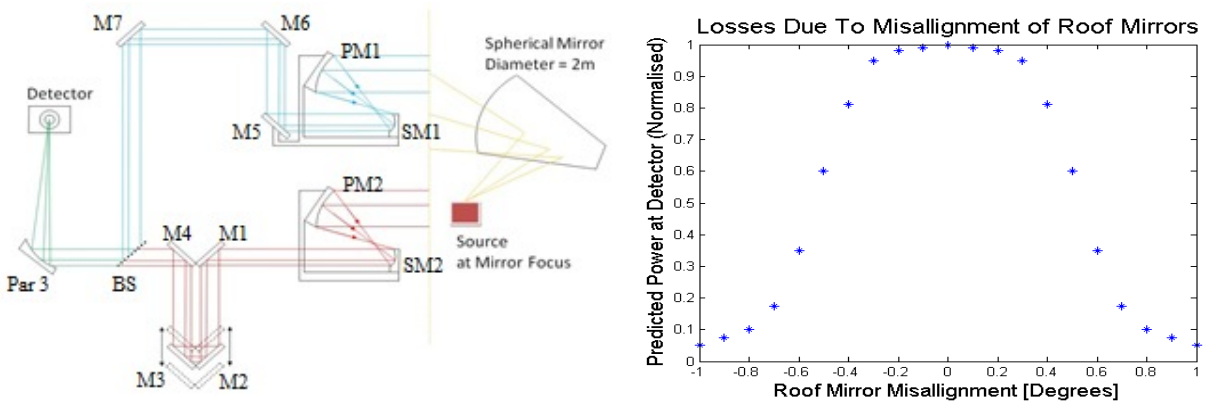

Figure 10. l*eft*: A schematic of the Cardiff testbed The blue rays trace out the spatial arm, where the condensing optics PM1 and SM1 (and the flat M5) move across the baseline of 100mm. The red rays trace out the spectral arm, where the condensing optics PM2 and SM2 are stationary, and the roof mirror (M2 and M3) move about the ZPD to record the interferoram. *Right*: Analysis of the levels of loss when an error is introduced into the angles of the roof mirror.

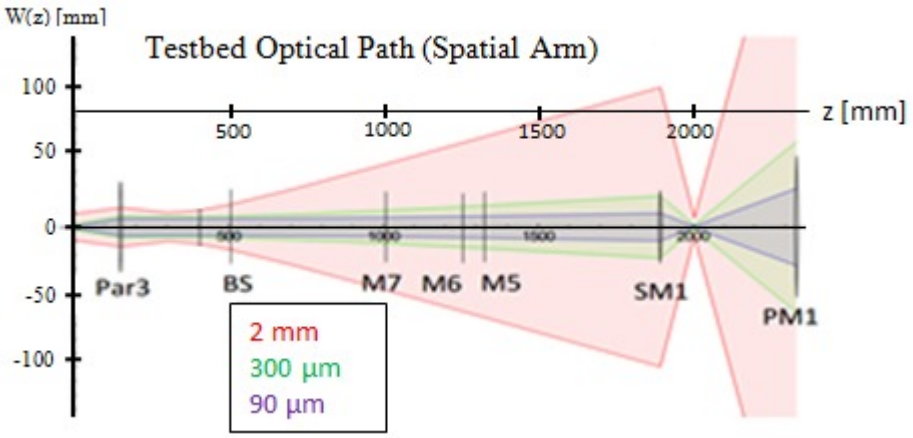

Figure 11. The beam path through the testbed, where a Gaussian beam was used to analyse the level of diffraction throughout the system for a number of wavelengths.

4.2 Far-Infrared Interferometer Instrument Simulator (FIInS)

The FISICA activities are further supported by a dedicated instrument simulator which was developed specifically for modelling the behavior of a double-Fourier instrument, and how such an instrument will measure both point source and extended source astronomical scenes [20]. The Far-Infrared Interferometer Instrument Simulator (FIInS) was developed by Roser Juanola-Parramon as part of her doctoral thesis [21]. The use of such an instrument simulator will help to lay the path for the software tools that will be required for data analysis of measurements from a future double-Fourier system.

4.3 Other FISICA Work

There are a range of other activities currently underway as part of the FISICA project [22], which involves many research institutes from across Europe, Canada, and the U.S. Such work includes studies of metrological problems and system requirements for a space-based far-IR interferometer [9], research into advanced carbon composite materials for novel light weight mirror designs [23], and of course detailed definition of the key science questions that can only be answered with a far-IR interferometer [24].

5. SUMMARY

Based on a trade-off analysis of a variety of telescope designs, and a number of variations of each design, using conventional ray tracing techniques, the current chosen baseline design for the light collecting telescopes for the proposed far-IR double Fourier interferometer is an on-axis Cassegrain with F/5 and de-magnification of m = 10-12. The design may be revised after the completion of ongoing physical optics simulations of the various designs. Expanding the wavelength range beyond 200 μm (i.e. including a band spanning 200 - 400 μm), or employing a wider field of view will undoubtedly also require a revision of the baseline design.

The tight restriction on visibility, based on the error budget set by the SPIRIT study [7], places stringent requirements on mirror surface accuracy, where surface form errors cannot exceed sizes of the order of 100's of nm (which will likely be very difficult to achieve). Surface roughness will also need to be well controlled if such high levels of visibility are to be achieved.

It has also been shown that the capability to model double Fourier testbeds can help to understand how to control potential losses, and how the limits of such systems can be predicted. Ongoing testbed measurements, and simulations of same, will help pave the way for building a future far-IR interferometer in space, as well as understanding how to analyse the complex data that will be produced from these novel double Fourier astronomical measurements.

Acknowledgements

The corresponding author wishes to acknowledge the contributions of the full FISICA Consortium [22] to the work presented in this paper.

The research leading to these results has received funding from the European Union's Seventh Framework Programme (FP7/2007 − 2013) under FISICA grant agreement no. 312818.

REFERENCES

[1] Kennedy, G. M., "Nature or nurture of coplanar Tatooines: the aligned circumbinary Kuiper belt analogue around HD 131511," Monthly Notices of the Royal Astronomical Society: Letters, Volume 447, Issue 1, pp. L75-L79, (2015).

[2] Servillat, M., Coleiro, A., Chaty, S., Rahoui, F. and Zurita Heras, J. A.,"Herschel observations of dust around the high-mass X-ray binary GX 301-2," The Astrophysical Journal, Volume 797, Issue 2, article id. 114, 10 pp., (2014).

[3] Oteo, I., "Dust correction factors over $0 < z < 3$ in massive star-forming galaxies derived from a stacking analysis of Herschel data," Astronomy & Astrophysics, Volume 572, id.L4, 12 pp., (2014).

[4] Werner, M., Fazio, G., Rieke, G., Roellig, T. L., Watson, D. M., "First fruits of the Spitzer Space Telescope: galactic and Solar system studies," Annual Review of Astronomy & Astrophysics, Volume 44, Issue 1, pp.269-321, (2006).

[5] Goicoechea, J., Isaak, K., Roelfsema, P., Spinoglio, L. and Swinyard, B., [The SPICA Assessment Study Report], Prepared by the ESA SPICA Study Team, the SPICA Telescope Science Study Team, the JAXA/ISAS SPICA Team and the SAFARI Consortium, (2011).

[6] Elias, N. M. II, Harwit, M., Leisawitz, D. and Rinehart, S. A. "The mathematics of double-Fourier interferometers," The Astrophysical Journal, Volume 657, Issue 2, (2007).

[7] Leisawitz, D. et al., "The Space Infrared Interferometric Telescope (SPIRIT): High-resolution imaging and spectroscopy in the far-infrared," Journal for Advanced Space Research, Volume 40, Issue 1, pp. 689-703, (2007).

[8] Helmich, F. P., Ivison, R. J., "FIRI - A far-infrared interferometer," Experimental Astronomy, Volume 23, Issue 1, pp. 245-276, (2009).

[9] Iafolla, V. A., Fiorenza, E., Iafolla, L., Lefevre, C., Magnafico, C., Santoli, F. and Spinoglio, L. "FISICA (Far Infrared Space Interferometer Critical Assessment) metrological problems and system requirements for interferometric observations from space," Metrology for Aerospace (MetroAeroSpace), 2014 IEEE, pp. 161-166, (2014).

[10] Zemax. "Zemax Support Literature: Getting Started Using ZEMAX,". http://www.radiantzemax.com/downloads/Getting_Started_With_Zemax_version2.1.pdf (25 January 2015).
[11] Xu, Y-L.," Fraunhofer diffraction of electromagnetic radiation by finite periodic structures with regular or irregular overall shapes," Journal of the Optical Society of America A, Vol. 32, Issue 1, pp. 12-21 (2015).
[12] Aime, C., Aristidi, E. and Rabbia, Y., "The Fresnel diffraction: A story of light and darkness," New Concepts in Imaging: Optical and Statistical Models, EAS Publications Series, Volume 59, pp. 37–58, (2013).
[13] Murphy, J. A. and Egan, A., "Examples of Fresnel diffraction using Gaussian modes," European Journal of Physics, Volume 14, Issue 3, pp. 121-125, (1993).
[14] Goldsmith, P. F., "Quasi-Optical Techniques," Proceedings of the IEEE, Volume 80, Issue 11, pp. 1729-1747, (1992).
[15] Baars, J. W. M., [The Paraboloidal Reflector Antenna in Radio Astronomy and Communication], Astrophysics and Space Science Library Volume 348, 87-88 (2007).
[16] ESA Concurrent Design Facility, "FIRI - Far Infrared Interferometer - CDF Study Report," Volume: CDF-49(A), pp. 130-131, (2006).
[17] Hyde, T. T., Leisawitz, D. T. and Rinehart, S., "System engineering the Space Infrared Interferometric Telescope (SPIRIT)," SPIE International Symposium on Optics and Photonics. UV Optical/IR Space Telescopes: Innovation Technologies and Concepts III; 24-27 Aug. 2007; San Diego, CA; United States, (2007)
[18] Ruze, J., "Antenna tolerance theory - a review," Proceedings of IEEE, Volume 54, Issue 4, pp. 633-640, (1966)
[19] Spencer, L.D., Naylor, D.A., Savini, G. and Ade, P.A.R., on behalf of the FISICA Consortium, " Spatial/spectral interferometry development for far-infrared space applications," IEEE Conference Publications, 39th International Conference on Infrared, Millimeter, and Terahertz waves (IRMMW-THz), pp. 1-2, (2014).
[20] Juanola-Parramon, R., Ade, P. A. R., Grainger, W. F., Griffin, M., Pascale, E., Savini, G., Spencer, L. and Swinyard, B., "A space-based far Infrared interferometer (FIRI) instrument simulator and test-bed implementation", Proceedings of SPIE 8550, Optical Systems Design, 85501Y (2012).
[21] Juanola-Parramon, R., "A far-infrared spectro-spatial space interferometer. Instrument simulator and testbed implementation", Doctoral thesis, UCL (University College London), (2014).
[22] Savini, G., on behalf of the FP7-FISICA Consortium, “FISICA-FP7,”,http://www.fp7-fisica.eu, (03 February 2015).
[23] Jones, M., on behalf of the FP7-FISICA Consortium, "Technical implications of CFRP mirrors at cryogenic (4K) temperatures," Online proceedings of the Second FISICA Workshop, Maynooth University, Kildare, Ireland, http://www.fisica2015.eu/programme.html , (05 February 2015).
[24] Spinoglio, L., Schito, D., Pezzuto, S. and Holland, W., on behalf of the FP7-FISICA Consortium, D1.1 Definition/update of key science questions and relevant data products: http://www.homepages.ucl.ac.uk/~ucapgsa/Test_docs/D1.1_submitted.pdf, (05 February 2015).